Walisongo Journal of Chemistry
Walisongo Journal of Chemistry Vol. 8 Issue 2 (2025), 218-241
ISSN: 2621-5985 (online); 2549-385X (print)
DOI: https://doi.org/10.21580/wjc.v8i2.26973

NICKEL-BASED CATALYSTS FOR UREA ELECTROLYSIS: A REVIEW OF ELECTROLYSIS PERFORMANCE AND CATALYST DESIGN

Raja Doli Tota Parulian Situmorang[1], Hernandi Sujono[1], Jasmansyah[2], Anceu Muniarti[2,3], Arie Hardian[2,3*], Ferli Septi Irwansyah[4]

[1]Department of Chemistry, Faculty of Sciences and Informatics, Universitas Jenderal Achmad Yani, Cimahi, West Java, Indonesia
[2]Study Program of Master of Chemistry, Faculty of Sciences and Informatics, Universitas Jenderal Achmad Yani, Cimahi, West Java, Indonesia
[3]Material and Environmental Development Center, Universitas Jenderal Achmad Yani, Cimahi, West Java, Indonesia
[4]Department of Chemistry Education, UIN Sunan Gunung Djati, Bandung, West Java, Indonesia

*Corresponding author: arie.hardian@lecture.unjani.ac.id

Abstract

The increasing concentration of urea in wastewater poses both an environmental challenge and an opportunity for sustainable hydrogen production through urea electrolysis, which depends on efficient electrocatalysts. This review focused on nickel-based catalysts due to their high catalytic activity and stability in alkaline media. Using the PRISMA method, twenty studies published between 2020 and 2025 were analyzed based on current density, cell potential, Tafel slope, and stability. Through thematic analysis, catalysts were categorized according to their structure, composition, design strategy, and performance at 10, 50, 100, and 500 mA cm^{-2}. The review also highlights the importance of testing catalysts in real wastewater rather than in idealized electrolytes. An effective catalyst should exhibit a porous or layered nanostructure, multimetallic composition, and surface doping, while avoiding noble metals and overly complex architectures that hinder charge transfer and scalability.

Keywords: *Catalytic Activity, Nickel-based Catalysts, PRISMA Method, Thematic Analysis, Urea Electrolysis*

Introduction

Urea is a nitrogen-rich compound commonly found in both industrial and domestic waste streams (Urbańczyk et al., 2016; Weerakoon et al., 2023). In industrial contexts, it is produced in large quantities and can enter aquatic environments through wastewater discharge from fertilizer and chemical manufacturing plants. In domestic settings, urea is the primary nitrogenous waste product in mammalian urine, originating from protein metabolism (Weerakoon et al., 2023). If untreated, urea can be hydrolyzed by urease enzymes into ammonia, which accelerates eutrophication by depleting dissolved oxygen levels and causes ecological imbalances and toxic effects in aquatic ecosystems (Shaban et al., 2024). The resulting nitrogen pollution has significant implications for environmental and public health (Masjedi et al., 2024).

Sustainable hydrogen production through urea electrolysis is an emerging strategy that offers dual benefits: environmental remediation and energy

generation. By replacing the energy-intensive oxygen evolution reaction (OER) at the anode in conventional water electrolysis with the more thermodynamically favorable urea oxidation reaction (UOR), the overall cell potential required is drastically reduced. The theoretical potential for urea electrolysis is only 0.37 V under standard conditions (Anuratha et al., 2022; Ge et al., 2023; J. Li et al., 2022). The corresponding reactions are as follows:

Urea Oxidation Reaction (UOR):

$CO(NH_2)_2(aq) + 6OH^- \rightarrow N_2 + 5H_2O(l) + CO_2(g) + 6e^-$; E° = −0.46 V vs. SHE (eq. 1)

Hydrogen Evolution Reaction (HER) in alkaline media (pH ≈ 14):

$6H_2O(l) + 6e^- \rightarrow 3H_2(g) + 6OH^-$; E° = −0.83 V vs. SHE (eq. 2)

Overall Reaction (UOR/HER):

$CO(NH_2)_2(aq) + H_2O \rightarrow N_2(g) + 3H_2(g) + CO_2(g)$; E° = 0.37 V (eq. 3)

Compared with the theoretical potential of 1.23 V for conventional water electrolysis, which consumes more energy, urea electrolysis is substantially more energy-efficient (X. Li et al., 2020). The corresponding reactions in water electrolysis are:

Oxygen Evolution Reaction (OER):

$2H_2O_{(l)} \rightarrow O_{2(g)} + 4H^+ + 4e^-$;
E° = +1.23 V (eq. 4)

Hydrogen Evolution Reaction (HER):

$4H^+ + 4e^- \rightarrow 2H_2(g)$;
E° = 0.00 V (eq. 5)

Overall Reaction (OER/HER):

$2H_2O\ (l) \rightarrow 2H_2(g) + O_2(g)$;
E° = 0.37 V (eq. 6)

Furthermore, urea electrolysis provides a valuable pathway for decentralized hydrogen production while simultaneously reducing harmful nitrogen-based pollutants in wastewater streams.

Nickel-based catalysts are among the most extensively studied materials for urea electrolysis due to their favorable electronic configuration, redox flexibility, affordability, and strong affinity for urea and hydroxide intermediates (Vij et al., 2017). These catalysts exhibit high electrocatalytic activity and durability under alkaline conditions, making them ideal candidates for practical UOR–HER systems (Anuratha et al., 2022; Ge et al., 2023; J. Li et al., 2022). Various modification strategies, such as incorporating secondary or tertiary metals, phosphidation, or supporting on high-surface-area substrates, have been explored to further enhance their catalytic properties (Anuratha et al., 2022; Ge et al., 2023; J. Li et al., 2022).

Despite these advances, there remains a lack of systematic comparative analysis linking synthesis methods, catalyst architecture, and electrochemical performance under standardized testing conditions. Existing reviews often emphasize mechanistic insights or material characterization without comprehensively benchmarking performance metrics. For instance, (Tumiwa & Mizik, 2025) primarily discusses cost-efficiency processes for urea electrolysis but provides a limited comparison of catalyst performance. (Ge et al., 2023) focuses on mechanistic aspects and characterization techniques but excludes studies beyond 2023. Similarly, (Anuratha et al., 2022) considers catalyst design and performance but lacks a current-density-based benchmarking approach and only covers studies published up to 2021. (J. Li et al., 2022) prioritizes structural and morphological analyses without integrating recent literature or correlating these features to cell performance, covering studies only up to 2022.

In contrast, this review presents a performance-driven evaluation of nickel-based catalysts for urea electrolysis by integrating structural and electrochemical parameters. Studies published between 2020 and 2025 were selected through the PRISMA (Preferred Reporting Items for Systematic Reviews and Meta-Analyses) framework and evaluated based on reported current densities, cell potentials, Tafel slopes, turnover frequencies, and stability under alkaline urea conditions. Through thematic analysis, the review systematically

classifies and compares nickel-based catalysts according to their structural features, design strategies, compositions, and performance at key current density benchmarks (10, 50, 100, and 500 mA cm^{-2}). This approach provides practical insights and identifies emerging trends in high-performance urea catalysts. The analysis also considers real-world electrolyte limitations, particularly the discrepancy between idealized test solutions and actual urea-containing wastewater, to propose a more realistic framework for future catalyst development.

Experimental section

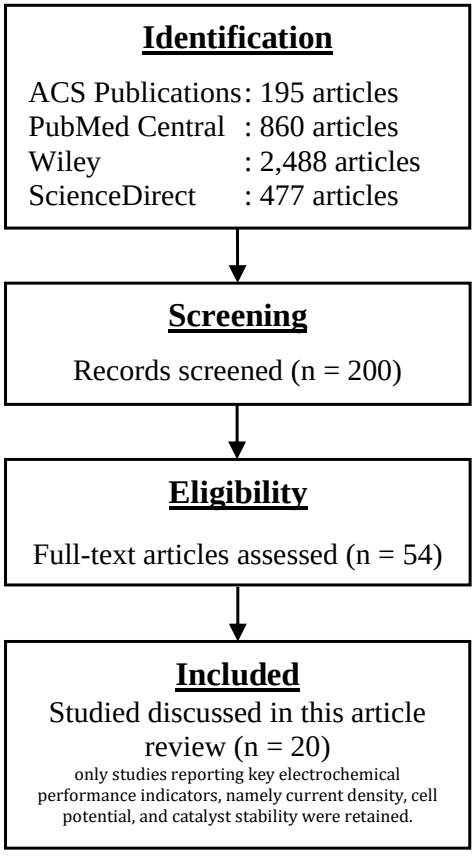

Figure 1. Flow diagram summary of literature review using PRISMA Method

This review employed a systematic literature search guided by the PRISMA approach. **Figure 1** illustrates the key stages of this review following the PRISMA framework. The initial identification phase involved keyword-based filtering using the term "Nickel-Based Catalyst for Urea Electrolysis," limited to publications from 2020 to 2025 and restricted to the "research article" type. The databases searched included ACS Publications, PubMed Central, Wiley Online Library, and ScienceDirect.

Due to access limitations, only open-access articles were included; subscription-based content from ScienceDirect was excluded at this stage. The initial number of articles identified from each database was as follows: ACS (195 articles), PubMed Central (860 articles), Wiley (2,488 articles), and ScienceDirect (477 articles), yielding a total of 4,020 articles.

In the screening phase, the top 50 results from each database were selected based on relevance, as articles beyond this threshold were generally outside the scope of this review. This step produced a pool of 200 articles. Abstracts were subsequently reviewed to ensure alignment with the review's focus on UOR and HER, specifically involving nickel as the primary catalytic component. This screening process narrowed the selection to 54 articles.

During the inclusion phase, only studies reporting key electrochemical performance indicators, namely current density, cell potential, and catalyst stability, were retained. This final selection resulted in 20 articles deemed suitable for detailed comparative analysis. The distribution of these included articles by database source was: ACS (2 articles), PubMed Central (4 articles), Wiley (13 articles), and ScienceDirect (1 article) (Alex et al., 2024; Dharmaraj et al., 2024; Fan et al., 2024; Gao et al., 2023; Gómez-Sacedón et al., 2024; Huang et al., 2024; Jin et al., 2024; X. Li et al., 2024; Ma et al., 2024; Miao et al., 2024; Parvin et al., 2024; Qian et al., 2023, 2024; Shaarawy et al., 2024; H. Wang et al., 2021; Y. Wang et al., 2023; Yang et al., 2024; Yun et al., 2021; Y. Zhao et al., 2024; Zhong et al., 2022).

The selected articles were further categorized based on their catalyst synthesis methods, material compositions, and performance specifications to identify respective advantages and limitations. A comparative analysis was then conducted, focusing on key parameters such as current density, cell potential, Tafel slope, turnover

frequency (TOF), and operational stability. Catalysts were grouped and discussed according to trends in architecture, compositional synergy, and electrolyte conditions, supported by relevant references. The best-performing systems at benchmark current densities (10, 50, 100, and 500 mA cm^{-2}) were systematically identified. This methodological framework is reflected in the Results and Discussion.

Results and Discussion

To provide a structured and comparative overview of the selected nickel-based catalysts, **Table 1** summarizes the 20 most relevant systems reported between 2020 and 2025. These catalysts were chosen based on the clear reporting of key performance metrics, including cell potential, current density, and stability. Additionally, supporting parameters such as the Tafel slope and TOF, when available, were included to enable a comprehensive comparison of kinetic behavior and catalytic efficiency. This tabulation serves as the foundation for the detailed analyses discussed in **Sections 3.1 to 3.9**, where performance trends and structure–function relationships are critically evaluated.

Table 1. Electrochemical Performance of Selected Catalysts

Catalyst	Description	Anode/Cat-hode	Current Density ($mA \cdot cm^{-2}$)	Cell Potential (V)	Tafel Slope ($mV \cdot dec^{-1}$)	TOF	Stability (h)	Ref.
Mo_3P@NiCoP/NF	Molybdenum-doped nickel–cobalt phosphide nanostructures on nickel foam	Catalyst itself	10	1.285	134.01	–	12	(X. Li et al., 2024)
S-doped $Ni(OH)_2$/Cu	Sulfur-doped $Ni(OH)_2$ on Cu composite	Catalyst itself	10	1.35	27	–	32	(Fan et al., 2024)
P–NiFe@CF	Phosphorized nickel–iron alloy on acid-treated carbon felt	Catalyst itself	10	1.37	107.2	–	8	(Yun et al., 2021)
$MoNi_4$/NiO heterostructure	$MoNi_4$ alloy and nickel oxide heterojunction on nickel foam	Catalyst itself	10	1.41	48	0.44	54	(Y. Zhao et al., 2024)
Tailored $Ni(OH)_2$/CuCo/$Ni(OH)_2$ Composite	Sandwich-like $Ni(OH)_2$/CuCo composite interfaced with NiMo	$Ni(OH)_2$/CuCo/$Ni(OH)_2$ (anode) and NiMo (cathode)	10	1.42	96	–	50	(Parvin et al., 2024)
Ni–BDC–t/NF	Nickel-based metal–organic framework (Ni–BDC) nanosheets on nickel foam	Ni–BDC 10/NF (anode) and Pt/C/NF (cathode)	50	1.53	19	–	11	(Huang et al., 2024)
NiCu–NF / a–NiMo–NF	Porous nickel–copper and amorphous nickel–molybdenum coatings on nickel felt	NiCu–NF (anode) and a–NiMo–NF (cathode)	50	1.6	–	–	120	(Dharmaraj et al., 2024)
Co–$Ni(OH)_2$	Cobalt-doped nickel hydroxide on Pt/C substrate	Pt/C	100	1.357	24.7	–	100	(Y. Wang et al., 2023)
($Ni(OH)_2$–Ni@CNT)	Nickel hydroxide-coated Ni nanoparticles	Nickel oxyhydroxide-modified Ni (anode, 20	100	1.36	30	0.5	60	(Alex et al., 2024)

Catalyst	Description	Anode/Cat-hode	Current Density ($mA \cdot cm^{-2}$)	Cell Potential (V)	Tafel Slope ($mV \cdot dec^{-1}$)	TOF	Stability (h)	Ref.
	embedded in carbon nanotubes	cm^2) and Pt foil (cathode, 25 cm^2)						
NiS Nanotubes	Nickel sulfide nanotubes	NiS Nanotubes (anode) and Pt/C (cathode)	100	1.39	23.62	0.17	10	(Zhong et al., 2022)
Pt–NiFeP/NF	Pt nanoparticles decorated on NiFeP/NF	Catalyst itself	100	1.41	47.7	–	40	(Miao et al., 2024)
NiFeO/NiFe	NiFe oxide bilayer on a metallic NiFe layer	NiFeO (anode) / NiFe (cathode)	100	1.43	104	–	5 (from 300 min conversion)	(Gómez-Sacedón et al., 2024)
Ru–NiO/p–Ni	Ruthenium-doped nickel oxide nanosheets on porous nickel	Catalyst itself	100	1.58	45.28	–	100	(Jin et al., 2024)
NiFeMo-based catalyst	Layered NiFeMo alloy nanosheets on nickel foam	Ru–NiFeMo (cathode) and NiFeMo 811 (anode)	100	1.58	16.77	–	60	(Ma et al., 2024)
Ni_2P@Ni–MOF/NF	Nickel phosphide nanolayer on Ni–MOF grown on nickel foam	Catalyst itself	100	1.65	43.8	–	20	(H. Wang et al., 2021)
NI-P Nanosheets	Ultrathin circular Ni–P nanosheets	Catalyst itself	109.75	1.52	22.56	–	70	(Yang et al., 2024)
Ni–SO_x	Sulfur-modified nickel surface film	Catalyst itself	323.4	1.65	–	–	80	(Gao et al., 2023)
CoNi coupled with CoNiMoO	CoNi alloy coupled with CoNiMoO nanoparticles on nickel foam	Catalyst itself	500	1.58	30	–	120	(Qian et al., 2023)
N–Ni–MoO_2/NF	Nitrogen-doped Ni–MoO_2 nanosheets on nickel foam	Catalyst itself	500	1.753	38.69	–	100	(Qian et al., 2024)
Ni–Co–nano–graphene thin film	Nickel–cobalt–nanographene composite coating on carbon steel	Ni–Co–nano–graphene (cathode) between two pure Ni anodes	700	1.75	–	–	50	(Shaaraw y et al., 2024)

Catalyst Architecture and Morphology

Catalyst architecture and surface morphology are critical parameters in enhancing electrochemical performance during urea electrolysis. The overall design determines the number of accessible active sites and mass-transport characteristics, local reaction environments, and long-term stability. Among the 20 studied systems, a clear trend emerged across four key structural categories.

Nanostructured Arrays and Porous Architectures

Several high-performing catalysts employed porous architectures to maximize surface accessibility, often by using nickel

foam as a conductive and structurally stable base, as illustrated in **Figure 2** and **Figure 3**. For instance, the $MoNi_4/NiO$ heterostructure ($MoNi_4/NiO$ on Ni foam) exhibited excellent performance with a low cell potential of 1.41 V at 10 mA cm^{-2} and a Tafel slope of 48 mV dec^{-1} (Y. Zhao et al., 2024). This nanosheet-array design provides abundant exposed edges for urea oxidation and enables fast charge transfer across the heterointerface (L. Chen et al., 2024; Ji et al., 2020). The intimate contact between $MoNi_4$ and NiO likely promotes synergistic effects and local electric-field modulation at the interface, facilitating the adsorption and deprotonation steps in the urea oxidation reaction (Bao et al., 2023; Y. Zhao et al., 2024).

Nanostructured Arrays and Porous Architectures

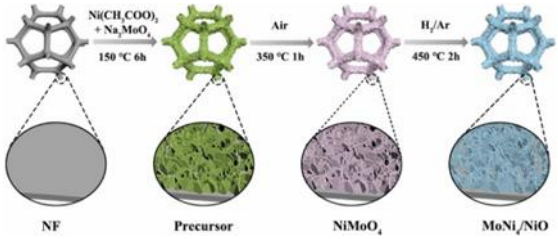

Figure 2. Synthesis of $MoNi_4/NiO$ heterostructure (Y. Zhao et al., 2024)

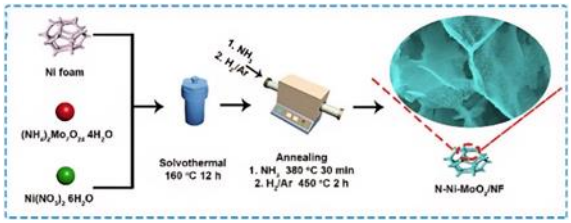

Figure 3. Synthesis of N–Ni–MoO_2/NF (Qian et al., 2024)

Similarly, nitrogen-induced Ni–MoO_2 micro/nanoarrays on nickel foam (N–Ni–MoO_2/NF) demonstrated how engineered array morphologies could sustain high current densities up to 500 mA cm^{-2} while maintaining a moderate cell voltage of 1.753 V and a competitive Tafel slope of 38.69 mV dec^{-1} (Qian et al., 2024). The hierarchical array promotes bubble release and minimizes diffusion limitations at elevated operational rates (K. Chen et al., 2024). Moreover, nitrogen doping via NH_3 treatment (see **Figure 3**) introduces compressive strain and modulates the electronic structure, contributing to stable performance over 100 hours (Qian et al., 2024).

Another representative example is Mo_3P@NiCoP/NF (X. Li et al., 2024), which combined phosphide functionality with a porous bimetallic surface. This architecture enabled hydrogen evolution and urea oxidation to proceed at a notably low onset potential (1.285 V at 10 mA cm^{-2}), although the relatively high Tafel slope indicates limited interfacial charge-transfer efficiency. In this regard, the large electrochemically active surface area (ECSA) of the porous Ni foam primarily affected cell voltage, while the kinetics remained governed by the local electron density at the active metal sites.

The Ru–NiO/p–Ni catalyst (Jin et al., 2024) also benefitted significantly from a nanostructured porous framework, achieving long-term operational stability exceeding 100 hours. While Ru doping improved conductivity and bifunctionality, the porous nickel substrate maintained ion flow and structural robustness at higher currents. Both stability and cell potential were thus enhanced by the porous backbone. Chemically, such nanostructures influence electric double-layer formation and preserve local OH^- and urea concentrations near active sites, while porosity increases the number of accessible reaction sites.

Hollow and Tubular Structures

Hollow and tubular morphologies have been explored to further enhance catalytic activity by improving bubble release and exposing inner and outer active surfaces. These structures mitigate concentration polarization and facilitate efficient mass transport.

As illustrated in **Figure 4**, the NiS catalyst synthesized via electrospinning adopted a nanotubular structure. Such hollow architectures provide a high internal surface area that allows deep electrolyte penetration and mechanical resilience. NiS

nanotubes, used as anodes in conjunction with Pt/C cathodes, exhibited a Tafel slope of 23.62 mV dec^{-1} and a TOF of 0.17 s^{-1} (Zhong et al., 2022), indicating a highly active and accessible catalytic surface.

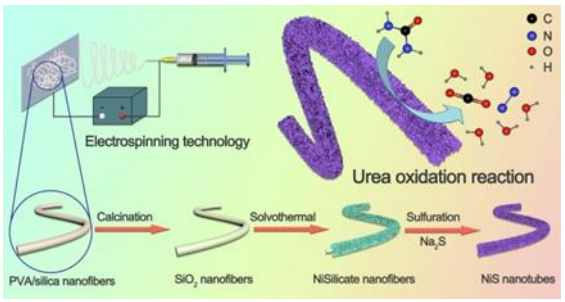

Figure 4. Synthesis of N–Ni–MoO_2/NF (Zhong et al., 2022)

In another example, ($Ni(OH)_2$)–Ni@CNT (Alex et al., 2024) embedded hydroxide-coated nickel nanoparticles within carbon nanotubes. This hybrid structure combined hollow internal channels (from CNTs) with a chemically active hydroxide shell. The configuration allowed rapid charge transport along the CNTs while exposing $Ni(OH)_2$ surfaces to urea molecules through external and internal access points. It supported sustained operation at 100 mA cm^{-2} and exhibited excellent stability over 60 hours, underscoring the advantage of chemically compatible tubular frameworks. The hollow-tubular form enhanced ion diffusion and accommodated gas evolution more effectively than dense particles. Furthermore, NiS offers intrinsic urea-oxidation activity owing to its distinctive d-band structure, which facilitates stronger interactions with urea-derived intermediates (Aladeemy et al., 2025; Wu et al., 2020; Q. Zhao et al., 2021).

Layered Nanosheets and Two-Dimensional (2D) Morphologies

Two-dimensional nanosheet structures, particularly those vertically aligned on conductive scaffolds, emerged as a recurring design. For instance, Ni–BDC–t/NF, a morphology-controlled nickel–organic framework converted into thin nanosheets on nickel foam, exhibited a moderate Tafel slope of 19 mV dec^{-1} and a cell potential of 1.53 V (Huang et al., 2024). The flat yet porous morphology maximized the exposure of metal–organic coordination sites (Ghosh et al., 2023), while the underlying nickel foam ensured efficient charge transport (Huang et al., 2024; Hu et al., 2019).

The selected area electron diffraction (SAED) pattern of Ni@CNT, shown in **Figure 5**, revealed diffraction spots corresponding to the (002) plane of graphitic CNTs, indicative of a layered carbon structure, and the (111) plane of metallic Ni, characteristic of its face-centered cubic (fcc) lattice. In contrast, the $Ni(OH)_2$–Ni@CNT sample additionally exhibited diffraction from the (100) and (110) planes of β-$Ni(OH)_2$, confirming the successful formation of crystalline nickel hydroxide on the Ni surface.

A particularly notable configuration was the $Ni(OH)_2$–Ni@CNT system, which integrated chemically activated carbon nanotubes with nickel hydroxide layers (Alex et al., 2024). This hybrid anode–cathode system achieved a competitive TOF of 0.5 s^{-1} and a Tafel slope of 30 mV dec^{-1}. The CNT network likely served as a conductive scaffold that mitigated Ni nanoparticle agglomeration and enhanced electron transport across the electrode (Alex et al., 2024; Islam Rubel et al., 2019; Tutar et al., 2024). Meanwhile, the *in situ* generation of $Ni(OH)_2$ continuously replenished active sites during operation, ensuring sustained catalytic performance over 60 hours.

Another representative system was the NiFeMo-based catalyst (Ma et al., 2024), consisting of alloyed nanosheets deposited on nickel foam. Its superior activity arose from its two-dimensional morphology and trimetallic composition. The sheet-like structure promoted intimate contact with the electrolyte, while the incorporation of Mo into the NiFe matrix enhanced conductivity and optimized energy-band alignment. Fe facilitated OH^- adsorption, a key intermediate step in urea oxidation, while Ni served as the primary active site responsible for urea molecule cleavage (Alex et al., 2024; Islam Rubel et al., 2019; Ma et al., 2024; Tutar et al., 2024).

This design significantly improved reaction kinetics, reflected in a remarkably low Tafel slope of 16.77 mV dec^{-1} at 100 mA cm^{-2}, one of the best performances among the reviewed catalysts (Ma et al., 2024). The reduced slope indicates accelerated charge-transfer kinetics and underscores the importance of structural exposure in promoting catalytic reactions. Moreover, the robust nanosheet framework maintained mechanical stability over extended testing periods, even under industrial-level current densities.

In summary, layered nanosheet morphologies primarily contribute to reducing the Tafel slope and enhancing long-term durability, owing to their high density of exposed active sites and synergistic interactions within the alloyed lattice.

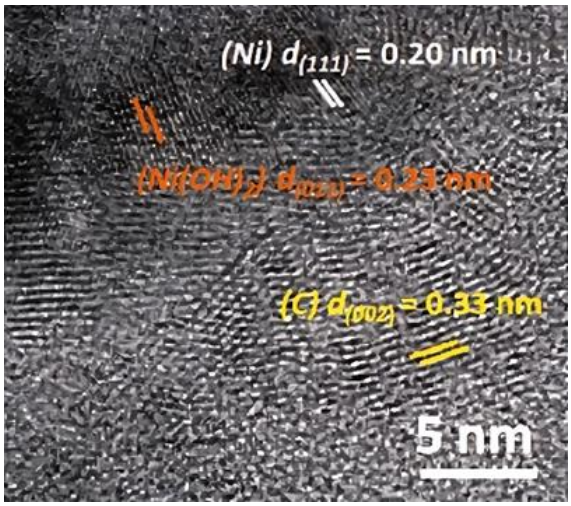

Figure 5. TEM image of N–Ni–MoO_2/NF (Alex et al., 2024)

Composite Layered Interfaces and Core–Shell Designs

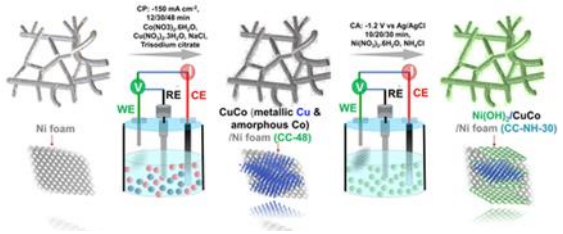

Figure 6. Preparation of $Ni(OH)_2$/CuCo/$Ni(OH)_2$ composite (Parvin et al., 2024)

Advanced composite architectures, such as the tailored $Ni(OH)_2$/CuCo/$Ni(OH)_2$ system shown in **Figure 6**, illustrate how layering different transition-metal hydroxides could modulate local electron density and reaction pathways (Parvin et al., 2024). This composite configuration achieved a Tafel slope of 96 mV dec^{-1} and a low cell potential of 1.42 V at 10 mA cm^{-2}. The electrode operated stably for 50 hours, highlighting the value of composite layering and Cu–Co interfacial synergy. However, the relatively high Tafel slope (96 mV dec^{-1}) suggests sluggish charge transfer, likely due to the dense hydroxide layers limiting ionic diffusion (L. Li et al., 2024; Nagappan et al., 2023; Parvin et al., 2024).

Although not the most kinetically active catalyst, this configuration demonstrates how interfacial charge redistribution and modified adsorption properties could arise from the CuCo intermediate layer (Parvin et al., 2024). Similarly, the Ni_2P@Ni–MOF/NF system represents a core–shell configuration in which phosphide nanoparticles are encapsulated within a metal–organic framework (MOF) shell (H. Wang et al., 2021). This structure exhibited solid performance, with a Tafel slope of 43.8 mV dec^{-1} at a cell potential of 1.65 V (100 mA cm^{-2}), likely attributable to the synergistic interaction between the conductive Ni_2P core and the porous MOF shell. The latter maintained electrolyte accessibility while preventing particle aggregation and metal leaching (Patel et al., 2023; H. Wang et al., 2021).

Bimetallic and Trimetallic Systems

The rational design of bimetallic and trimetallic catalysts has emerged as a compelling strategy to optimize UOR and HER. Their superior performance derives from the ability of multiple metal centers to modulate electronic structures, increase active-site density, and tailor reaction pathways. Among the reported systems, layered NiFeMo alloy nanosheets grown on nickel foam exemplified a high-performing trimetallic platform (Ma et al., 2024).

In this system, Ni served as the primary conductive backbone, while Fe and Mo tuned the surface chemistry and reaction

energetics. The catalyst achieved a cell voltage of 1.58 V at 100 mA cm^{-2} with an exceptionally low Tafel slope of 16.77 mV dec^{-1}, reflecting highly favorable reaction kinetics. The nanosheet morphology contributed to efficient charge transport, while Mo likely modified the *d*-band center, facilitating intermediate desorption (Ma et al., 2024; G. Wang et al., 2025). The use of nickel foam as a substrate further enhanced electrical conductivity and provided a porous scaffold that maximized catalyst utilization (Ma et al., 2024).

Similarly, the CoNi/CoNiMoO hybrid system exhibited impressive performance, sustaining 500 mA cm^{-2} at 1.58 V with a low Tafel slope of 30 mV dec^{-1} and high durability (120 h) (Qian et al., 2023). The CoNi base alloy provided synergistic catalytic activity for UOR, while Mo incorporation enhanced HER facilitation and overall bifunctionality. The architecture supports high current density and suggests that the ternary composition not only optimizes active-site energetics but also suppresses catalyst deactivation during prolonged operation (Qian et al., 2023).

The NiCu–NF and amorphous NiMo–NF coupled system also illustrates the strength of multimetallic synergy (Dharmaraj et al., 2024). Although structural details were limited, the pairing of a NiCu-based anode with an amorphous NiMo cathode achieved a cell potential of 1.60 V at 50 mA cm^{-2} and demonstrated excellent stability over 120 hours. The amorphous NiMo phase likely provided a high density of surface defects and active edge sites beneficial for HER, while the NiCu alloy anode promoted UOR activity and corrosion resistance (Dharmaraj et al., 2024; Santos et al., 2020). This finding emphasizes that amorphization, combined with compositional pairing, could yield enhanced electrocatalytic behavior without requiring crystallinity.

In a simpler binary configuration, the Pt–NiFeP/NF catalyst demonstrates the integration of a noble metal with a transition-metal phosphide matrix (Miao et al., 2024). Despite incorporating Pt, the system achieved a moderate cell potential of 1.41 V at 100 mA cm^{-2} with a Tafel slope of 47.7 mV dec^{-1}. This performance suggests a bifunctional role, where Pt accelerated HER while the NiFeP phase supported UOR. However, the average performance underscores that noble-metal inclusion alone does not guarantee superior activity, especially in the absence of strong structural or interfacial synergy.

Finally, the Co–Ni$(OH)_2$ catalyst on Pt/C exhibited strong binary performance, operating at 1.357 V for 100 mA cm^{-2} with a Tafel slope of 24.7 mV dec^{-1} and maintaining stability over 100 hours (Y. Wang et al., 2023). The system benefited from the high conductivity of Pt/C and the redox flexibility of Co–Ni hydroxides. The low Tafel slope indicates favorable reaction kinetics, likely due to efficient charge redistribution between Co and Ni centers (Gaur et al., 2023; Y. Wang et al., 2023). Nevertheless, the reliance on Pt limits scalability and cost efficiency, reinforcing the need for more earth-abundant alternatives.

In general, bimetallic and trimetallic catalysts exerted the most pronounced influence on Tafel slope and cell potential through synergistic effects on surface energetics and reaction kinetics. Across these multimetallic systems, a consistent advantage emerged from compositional synergy combined with rational structural design. However, performance did not always correlate with compositional complexity: Pt-containing systems did not automatically outperform non-noble counterparts, and structural optimization often proved as critical as elemental selection. Future research should therefore prioritize elucidating the mechanistic roles of individual metals within the catalytic cycle rather than relying solely on compositional diversity.

Phosphidation and Other Post-Treatments

Post-synthetic surface modifications, particularly phosphidation, have emerged as pivotal strategies for converting conventional transition-metal precursors into highly active electrocatalysts for urea electrolysis. These treatments alter the

surface electronic structure and introduce catalytically favorable phases, such as metal phosphides, which are known for their enhanced conductivity, stability, and bifunctionality in UOR and HER.

The Mo_3P@NiCoP/NF catalyst exemplifies an engineered phosphide composite that integrates molybdenum phosphide nanoparticles within a NiCoP matrix on nickel foam (X. Li et al., 2024). Operating at a relatively low cell potential of 1.285 V at 10 mA cm^{-2} and a high Tafel slope of 134.01 mV dec^{-1}, this system demonstrated moderate reaction kinetics despite its low onset potential.

As illustrated in **Figure 7**, phosphidation significantly enhanced the performance of nickel-based catalysts compared with their untreated counterparts. This improvement likely facilitated charge transfer and accelerated water dissociation during HER (W. Li et al., 2022; X. Li et al., 2024; Putri et al., 2023), while the NiCoP dual-metal base promoted efficient UOR activity. The use of nickel foam as a substrate further contributed to electrochemical stability by providing a mechanically robust, conductive, and porous framework (Poimenidis et al., 2023; Ratsoma et al., 2023).

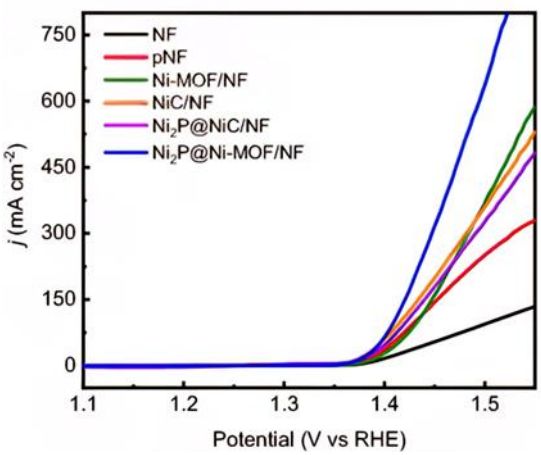

Figure 7. Voltage vs. RHE comparison between phosphidated and non-phosphidated nickel catalysts (H. Wang et al., 2021)

The P–NiFe@CF catalyst (Yun et al., 2021) employed a similar phosphidation approach on a NiFe alloy supported by acid-treated carbon felt. Although it achieved moderate performance, its operational stability was limited to approximately 20 hours at 50 mA cm^{-2}, likely due to incomplete phase conversion or weak interfacial adhesion of the phosphide layer.

Ni–P Nanosheets (Yang et al., 2024) offer another example of phosphidized structures. Their circular morphology maximizes active-site exposure; however, without strong compositional synergy, the resulting kinetic performance remains modest.

In contrast, S-doped $Ni(OH)_2$/Cu (Fan et al., 2024), though not phosphidized, demonstrates how alternative post-treatment strategies, such as sulfur doping, could achieve comparable benefits. Sulfur incorporation increased electrical conductivity and modulated the local electronic environment around nickel active centers. This catalyst performed effectively at 10 mA cm^{-2}, requiring only 1.35 V, and remained stable for 32 hours, underscoring that non-phosphide dopants could also yield substantial catalytic enhancement.

Similarly, Ni_2P@Ni–MOF/NF synthesized via phosphidation of a nickel-based metal–organic framework, exemplified the transformation of an ordered, porous structure into a catalytically active composite (H. Wang et al., 2021). Operating at 1.65 V (100 mA cm^{-2}) with a Tafel slope of 43.8 mV dec^{-1}, this catalyst benefited from dual advantages: (1) the formation of conductive Ni_2P active species, and (2) the preservation of the MOF's hierarchical porosity, which supported efficient mass transport and abundant active-site exposure (W. Li et al., 2022; X. Li et al., 2024; Putri et al., 2023) This combination of structural integrity and enhanced electronic activity represents a hallmark of successful post-synthetic treatments.

Phosphorus incorporation also played a key role in the P–NiFe@CF system, which achieved a low cell potential (1.37 V at 10 mA cm^{-2}) and a high Tafel slope (107.2 mV dec^{-1}) but exhibited limited stability (8 h) (Yun et al., 2021). The NiFe bimetallic composition benefited from electronic coupling between redox-active centers,

while phosphorus doping introduced new surface states that enhanced conductivity and optimized the binding energies of reaction intermediates (Putri et al., 2023). Nevertheless, the elevated Tafel slope suggests sluggish UOR kinetics, possibly due to incomplete phosphidation or the persistence of residual oxide layers that hinder electron transfer.

Even catalysts not explicitly categorized as phosphides, such as Pt–NiFeP/NF (Miao et al., 2024) and Mo_3P@NiCoP/NF (X. Li et al., 2024), exemplified the versatility introduced by phosphidation. The incorporation of phosphorus reduced the activation energy for HER by improving hydrogen adsorption ($H*$) and fine-tuning the electronic environment of transition-metal centers (W. Li et al., 2022; Putri et al., 2023). Furthermore, metal phosphides typically exhibited superior corrosion resistance in alkaline media, contributing to extended operational longevity.

Another intriguing system, Ni–SO_x, demonstrates how sulfur-containing species could restructure nickel active sites and selectively suppress water oxidation (Gao et al., 2023). Although synthesis details remained limited, its ability to sustain high current densities (323.4 mA cm^{-2} at 1.65 V) suggests that the modified surface morphology supported rapid catalytic turnover (X. Ao et al., 2022; Qiao et al., 2024).

Overall, phosphidation and related post-treatment methods have proven to be transformative not only chemically but also functionally. Phosphorus incorporation enhanced electronic conductivity due to its high electronegativity and strong metal–P covalency. However, these modifications must be precisely controlled: over-phosphidation could produce insulating or passivating surface layers, while under-phosphidation led to incomplete phase transformation and reduced catalytic efficiency (W. Li et al., 2022; Putri et al., 2023). The most effective systems integrated phosphidation with strategic substrate selection, such as nickel foam or carbon felt. Ultimately, the synergy between the active phase, conductive support, and hierarchical morphology determined the overall catalytic performance.

Use of Noble Metals

Noble metals such as ruthenium (Ru) and platinum (Pt) have been incorporated into urea electrocatalysis systems to enhance charge-transfer kinetics and improve intrinsic activity at the electrode interface. Their high conductivity and strong affinity for reaction intermediates enable dual functionality in facilitating UOR and HER. The rationale for their inclusion is well established; Pt and Ru exhibit exceptional electrical conductivity, catalytic activity for HER, and strong synergistic interactions when coupled with transition metals (Liu et al., 2024). However, their high cost, scarcity, and limited sustainability pose serious challenges to long-term scalability (Yu et al., 2020).

The Ru–NiO/p–Ni catalyst (Jin et al., 2024) exemplified this approach, leveraging the synergistic interaction between Ru nanoparticles and NiO nanosheets supported on porous nickel. Ruthenium enhanced the adsorption and activation of OH^- species, a key step in initiating urea oxidation. This catalyst demonstrated stable operation exceeding 100 hours and performed efficiently at 100 mA cm^{-2}, although its Tafel slope remained moderate relative to non-noble alternatives. The primary advantage was not in lowering the cell voltage but in maintaining catalytic integrity and bifunctionality over extended operating periods.

Another representative system, Pt–NiFeP/NF (Miao et al., 2024), employs Pt nanoparticles supported on a phosphidized NiFe matrix. In this regard, Pt contributes a HER-active interface, making the material suitable for electrodes in a two-electrode urea electrolysis configuration. While its bifunctional activity is notable, the high cost and scarcity of platinum significantly restrict practical deployment. Furthermore, prolonged electrolysis under alkaline conditions can lead to Pt surface poisoning through adsorption of carbonaceous intermediates or leached urea fragments.

In many systems, Pt has been utilized primarily as a cathode material to facilitate HER, while more cost-effective transition-metal-based materials serve as anodes. For example, in the $Ni(OH)_2$–Ni@CNT system, a Pt foil cathode (25 cm^2) paired with a Ni-based anode achieved an overall cell voltage of 1.36 V at 100 mA cm^{-2} (Alex et al., 2024). Although this value was impressive, the performance largely reflected Pt's inherent HER advantage, which might obscure the true anodic efficiency of the paired Ni-based catalyst (Isik et al., 2024; Seo et al., 2025). Similarly, the Ni–BDC–t/NF framework, when coupled with a Pt/C/NF cathode, attained 1.53 V at 50 mA cm^{-2}, suggesting that the anodic contribution alone might be insufficient to sustain high-efficiency electrolysis without noble-metal assistance (Huang et al., 2024).

A more integrated approach involves embedding noble metals directly within the catalyst architecture to achieve noble–non-noble synergy. In Pt–NiFeP/NF, Pt nanoparticles were incorporated into or supported on the NiFeP framework, enhancing electron transfer and bifunctional performance (Miao et al., 2024). This system reported a cell potential of 1.41 V at 100 mA cm^{-2} and a Tafel slope of 47.7 mV dec^{-1}, indicative of accelerated reaction kinetics. Nevertheless, the long-term durability of noble-metal components remains a concern: even trace amounts of Pt are prone to selective poisoning, dissolution, or agglomeration under prolonged electrochemical operation in complex electrolytes (Chidunchi et al., 2024; Wallnöfer-Ogris et al., 2024).

NiS nanotube catalysts, though paired with Pt/C cathodes, achieved competitive performance (1.39 V at 100 mA cm^{-2}, Tafel slope 23.62 mV dec^{-1}, TOF 0.17 s^{-1}) (Zhong et al., 2022). The nanotubular architecture enhanced diffusion and active-site exposure (Agrawal et al., 2024; Ke et al., 2021; Zhong et al., 2022), indicating that the NiS anode contributed significantly to the overall catalytic activity, while Pt primarily facilitated HER at the cathode. This underscores a persistent challenge in the field: Pt is often retained as a benchmarking material, which complicates the evaluation of true bifunctional performance in non-noble catalysts.

From a design standpoint, noble metals also enable atomic-scale engineering, such as single-atom catalysts or alloying strategies, which can induce lattice strain, tune *d*-band centers, and promote charge redistribution (Da et al., 2023). In summary, noble metals remain a powerful yet problematic component in urea electrolysis. They deliver superior HER kinetics and interfacial charge-transfer efficiency (Niu et al., 2023), but their use can overshadow the intrinsic capabilities of the primary catalyst and undermine the scalability of the system. Future efforts should focus on either eliminating noble metals or incorporating them at trace, atomically dispersed levels that resist leaching and maximize atomic utilization.

Support Materials and Substrates

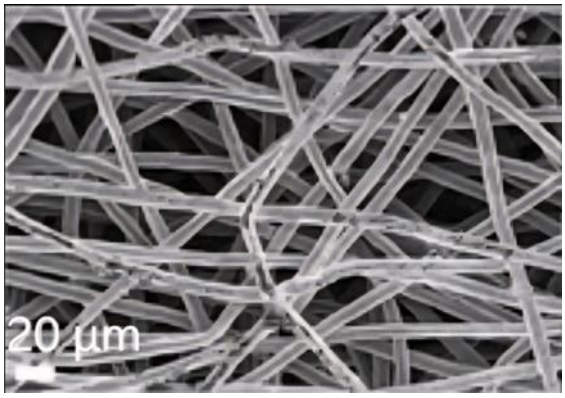

Figure 8. SEM image of cleaned nickel foam (NF) (Dharmaraj et al., 2024)

The choice of support material and substrate plays a critical role in determining the overall performance of urea electrolysis catalysts, serving not only as a mechanical platform but also as a component that governs morphology, electronic conductivity, wettability, active-site accessibility, and electrochemical stability (Moriau et al., 2021). Among the studies reviewed, nickel foam (NF) has been the most frequently employed support, followed by nickel felt, carbon-based materials, and, to

a lesser extent, copper and alloyed substrates.

As shown in **Figure 8**, cleaned nickel foam exhibits a well-defined three-dimensional porous morphology, offering an open framework that facilitates uniform catalyst deposition. This structural regularity enables intimate interfacial contact between the catalyst and the substrate while promoting efficient charge transfer and ion diffusion. Owing to its high porosity, superior electrical conductivity, and strong chemical stability in alkaline environments, nickel foam serves as a robust and reliable substrate for electrocatalyst development (G.-H. Ao et al., 2021; Poimenidis et al., 2023; Ratsoma et al., 2023). In some cases, NF also actively participates in catalysis, especially when transition-metal compounds are deposited or grown *in situ* on its surface. For instance, the Mo_3P@NiCoP/NF catalyst benefited significantly from the conductive NF scaffold (X. Li et al., 2024), achieving a low cell potential of 1.285 V at 10 mA cm^{-2}, despite a high Tafel slope of 134 mV dec^{-1}. This indicates that while the phosphide layer exhibited kinetic limitations, possibly due to surface reconstruction or sluggish charge transfer (Su et al., 2019), the NF substrate compensated by enhancing overall electron transport and gas diffusion (Poimenidis et al., 2023; Ratsoma et al., 2023).

Other systems, such as N–Ni–MoO_2/NF and Pt–NiFeP/NF, also demonstrate how NF supports improve performance through superior adhesion and structural integration (Miao et al., 2024; Qian et al., 2024). For example, the N-doped MoO_2 catalyst achieved a remarkably high current density of 500 mA cm^{-2} at 1.753 V, underscoring how the open-pore architecture of NF facilitated bubble release and mass transport under high reaction flux, even though the voltage remained relatively high (Qian et al., 2024).

In contrast, nickel felt, as used in the NiCu–NF / a–NiMo–NF system (Dharmaraj et al., 2024), offers a denser microstructure than NF while maintaining adequate porosity for gas and ion movement. Operating at 50 mA cm^{-2} for over 120 hours, the felt substrate provided excellent mechanical stability, making it suitable for long-term electrolysis applications.

On the other hand, carbon-based substrates offer advantages such as chemical inertness, high surface area, and lightweight structure, and are often used in the form of CNTs, graphene sheets, or carbon cloth. In the $Ni(OH)_2$–Ni@CNT catalyst, CNTs not only served as a conductive matrix but also helped to disperse Ni active species uniformly, lowering the Tafel slope to 30 mV dec^{-1} and achieving a respectable TOF of 0.5 s^{-1} (Alex et al., 2024). This hybrid system demonstrates how nanocarbon supports can reduce overpotentials by enhancing electronic conductivity and facilitating charge separation (Agrawal et al., 2024; Ke et al., 2021). Carbon felt was also used in P–NiFe@CF (Yun et al., 2021), enabling lighter and low-cost electrodes. While it increases surface area and provides chemical stability, its conductivity is generally lower than that of nickel-based substrates unless modified. This limitation often restricts the current response under industrial current densities.

A Pt/C substrate was utilized in Co–$Ni(OH)_2$ (Y. Wang et al., 2023). While the Pt/C base enhanced HER kinetics and charge transfer, it was susceptible to carbon degradation at higher voltages and could not withstand prolonged alkaline exposure. For this reason, its application remains mostly academic. Similarly, CoNi–CoNiMoO catalysts likely benefit from an internal conductive network, though the exact substrate is not specified (Qian et al., 2023). Given the high performance (1.58 V at 500 mA cm^{-2}), the underlying support might play a significant role in heat dissipation and mechanical durability, especially under intense current conditions.

There are also examples of non-traditional supports, such as CuCo/$Ni(OH)_2$ sandwich composites on copper mesh, where the metallic copper likely aids in uniform current distribution and provides synergistic interfacial effects between Cu and Ni species (Parvin et al., 2024). The resulting catalyst achieved 1.42 V at 10 mA cm^{-2}, and the high Tafel slope of 96 mV dec^{-1} indicates that the support might contribute

more to structural stability than to intrinsic reaction kinetics.

It is also worth noting that while support materials enhance performance, they can become unstable during long-term cycling, particularly if their surfaces passivate, delaminate, or corrode in harsh alkaline or urea-rich environments. Therefore, the chemical compatibility and interfacial bonding between the catalyst and support are as important as their electrical properties.

Catalyst Classification: Bifunctional vs. Monofunctional

A crucial perspective in evaluating urea electrolysis systems lies in distinguishing bifunctional catalysts, which catalyze both UOR and HER, from monofunctional systems, which are active predominantly toward one half-reaction. This classification is not merely semantic; it has profound implications for electrolyzer architecture, catalyst durability, and overall system efficiency.

Several of the reviewed catalysts exhibited bifunctionality. For instance, NiFeMo-based nanosheets supported on nickel foam showed compelling activity at the anode and cathode, achieving 1.58 V at 100 mA cm^{-2} with a remarkably low Tafel slope of 16.77 mV dec^{-1}, indicating rapid kinetics likely arising from synergistic electronic effects among Ni, Fe, and Mo (Ma et al., 2024; Qu et al., 2024). The fact that the same catalyst class can be used on both electrodes suggests balanced reaction rates and stability across both half-reactions, simplifying reactor design and enhancing cost-effectiveness.

Similarly, in the case of NiCu–a-NiMo/NF electrodes, the authors strategically paired a NiCu-based anode with an amorphous NiMo cathode, leveraging the redox flexibility of both systems (Dharmaraj et al., 2024). This design illustrates a semi-bifunctional approach, where metallic synergy and matched overpotentials improve full-cell integration. Achieving 1.6 V at 50 mA cm^{-2}, this system exemplifies how bifunctionality can be realized either within a single material or through complementarily designed electrode pairs.

In contrast, monofunctional catalysts focus on excelling at a specific half-reaction. For example, Ni-BDC-t/NF (Jin et al., 2024; Tumiwa & Mizik, 2025), used as the anode with Pt/C as the cathode, was tailored for efficient UOR, achieving a moderate cell voltage of 1.53 V at 50 mA cm^{-2} and a Tafel slope of 19 mV dec^{-1}. The use of Pt on the cathode side reflects a monofunctional strategy (Huang et al., 2024), where separate optimization pathways are pursued for UOR and HER. This approach offers advantages in fine-tuning surface interactions and catalyst specificity, though it increases system complexity and material costs due to the inclusion of noble metals.

Another monofunctional system involved a NiS nanotube-based anode paired with a Pt/C cathode, delivering 1.39 V at 100 mA cm^{-2} with a relatively low Tafel slope of 23.62 mV dec^{-1} and a measurable TOF of 0.17 s^{-1} (Zhong et al., 2022). The design was clearly optimized for UOR, while the cathodic side relied on the well-established HER performance of Pt-based materials (Zhong et al., 2022). Although effective, this approach may face scalability concerns due to its reliance on precious metals.

It is also worth noting that true bifunctional activity requires stable operation under oxidative and reductive potentials, which places considerable strain on structural stability and interfacial bonding. Materials such as Ni_2P@Ni-MOF/NF demonstrate potential in this regard, achieving 1.65 V at 100 mA cm^{-2} with a Tafel slope of 43.8 mV dec^{-1}, though their long-term durability under full-cell cycling remains underexplored (H. Wang et al., 2021).

In conclusion, bifunctional catalysts offer compact system design and cost advantages but often struggle to simultaneously optimize UOR and HER kinetics. In contrast, monofunctional systems allow for greater material specialization and potentially enhanced individual reaction performance, albeit with higher complexity and resource demands. A promising direction moving forward lies in

the rational design of bifunctional heterostructures or hybrid systems that combine the strengths of monofunctional specialization within a single integrated platform.

Performance Benchmarking Across Fixed Current Densities

A meaningful comparison of electrocatalysts for urea electrolysis requires not only performance at a single metric but also an integrated assessment across multiple current densities. This section compares the most promising catalysts operating at 10, 50, 100, and 500 mA cm^{-2}, prioritizing those with the lowest cell potential, followed by Tafel slope and operational stability. **Table 2** summarizes high-performing catalysts across a range of current densities (10–500 mA cm^{-2}), and the subsequent analysis explores correlations between synthesis methods, catalyst morphology, and electrochemical performance.

Table 2. Top-Performing Catalysts Across 10–500 mA cm^{-2}

Current Density (mA cm^{-2})	Best Catalyst (Cell Potential)	Best Catalyst (Tafel Slope)	Best Catalyst (Stability)
10	Mo_3P@NiCoP/NF (X. Li et al., 2024)	S-doped $Ni(OH)_2$/Cu (Fan et al., 2024)	$MoNi_4$/NiO heterostructure (Y. Zhao et al., 2024)
50	Ni-BDC-t/NF (Huang et al., 2024)	Ni-BDC-t/NF (Huang et al., 2024)	NiCu-NF/a-NiMo-NF (Dharmaraj et al., 2024)
100	Co-$Ni(OH)_2$ (Y. Wang et al., 2023)	NiFeMo-based (Ma et al., 2024)	Co-$Ni(OH)_2$ & Ru–NiO/p-Ni (Jin et al., 2024; Y. Wang et al., 2023)
500	CoNi–CoNiMoO (Qian et al., 2023)	-	CoNi–CoNiMoO (Qian et al., 2023)

Catalysts at 10 mA cm^{-2}

Lowest Cell Potential: Mo_3P@NiCoP/NF exhibited the best performance at 10 mA cm^{-2}, achieving a remarkably low cell potential of 1.285 V (X. Li et al., 2024). This phosphide-based heterostructure likely benefits from synergistic bimetallic interfaces between Mo, Ni, and Co. The high efficiency can be attributed to Mo doping, which enhances electrical conductivity and alters the surface charge distribution of the NiCoP matrix, allowing urea molecules to adsorb and oxidize more readily. However, the catalyst showed a relatively high Tafel slope (134 mV dec^{-1}), suggesting that the reaction kinetics remained sluggish and were likely limited by OH^- adsorption or intermediate desorption (X. Li et al., 2024; Poimenidis et al., 2023; Ratsoma et al., 2023).

Lowest Tafel Slope: S-doped $Ni(OH)_2$/Cu (Fan et al., 2024) demonstrated the lowest Tafel slope within this group, measured at 27 mV dec^{-1}. The incorporation of sulfur introduced defect sites, modifying the local electronic structure of $Ni(OH)_2$, making the surface more favorable for urea adsorption and charge transfer. This doping also reduced the energy barrier for the rate-determining dehydrogenation of adsorbed urea intermediates. However, the catalyst exhibited a slightly higher onset potential than Mo_3P@NiCoP/NF and only moderated operational stability.

Highest Stability: $MoNi_4$/NiO (Y. Zhao et al., 2024) offered the greatest stability at 10 mA cm^{-2}, maintaining continuous operation for 54 hours. This catalyst formed a stable heterojunction between a molybdenum–nickel alloy and nickel oxide, enabling efficient charge separation and enhancing the durability of active sites during extended electrolysis. Although it did not excel in voltage or kinetics, its layered interface mitigated rapid catalyst degradation and preserved surface reactivity under prolonged alkaline exposure.

Catalysts at 50 mA cm^{-2}

Lowest Cell Potential: Ni-BDC-t/NF achieved a modest cell potential of 1.53 V, which was notable given the use of an organic linker (BDC) with a conjugated aromatic backbone capable of facilitating π–d orbital interactions with Ni, thereby enhancing conductivity (Huang et al., 2024). However, its limited stability (11 h) suggests structural or chemical degradation during prolonged operation.

Lowest Tafel Slope: Ni-BDC-t/NF exhibited the most favorable kinetics with a Tafel slope of only 19 mV dec^{-1}, likely due to improved charge delocalization afforded by the biphenyl-dicarboxylic acid ligand (Huang et al., 2024).

Highest Stability: NiCu-NF/a-NiMo-NF demonstrated superior durability, maintaining stable performance for 120 hours. This robustness was attributed to the alloying of Ni with Mo and Cu, which inhibited surface passivation (Dharmaraj et al., 2024). Nonetheless, its cell potential (1.6 V) was not among the lowest, indicating possible kinetic limitations or elevated overpotentials resulting from its bulkier structure.

Catalysts at 100 mA cm^{-2}

Lowest Cell Potential: Both Co–$Ni(OH)_2$ and Ru–NiO/p–Ni achieved the lowest potentials of 1.36 V and 1.58 V, respectively (Jin et al., 2024), (Y. Wang et al., 2023), with Co–$Ni(OH)_2$ being more favorable in terms of energy efficiency. The layered hydroxide phase benefits from abundant OH^- adsorption and the presence of active Ni/Co sites, which synergistically enhance both OER and UOR (L. Li et al., 2024).

Lowest Tafel Slope: The NiFeMo-based catalyst outperformed others with a slope of only 16.77 mV dec^{-1}, indicating excellent charge-transfer properties. This finding can be attributed to its well-ordered alloy nanosheets, which minimize resistance and improve surface accessibility (Ma et al., 2024).

Highest Stability: Co–$Ni(OH)_2$ led in this category with 100 hours of stable operation, suggesting that its dual-metal hydroxide phase could provide structural resilience under continuous UOR conditions. Ru–NiO/p–Ni also maintained stability for 100 hours, reflecting the robustness of the NiO matrix and Ru's oxidation tolerance (Jin et al., 2024).

Catalysts at 500 mA cm^{-2}

Lowest Cell Potential: CoNi coupled with CoNiMoO exhibited the lowest cell potential (1.58 V) among high-current-density catalysts. The combination of CoNi and CoNiMoO likely generates a favorable interface that enhances catalytic synergy under high-demand conditions (Qian et al., 2023).

Highest Stability: The CoNi–CoNiMoO system remained stable for 120 hours, demonstrating superior robustness at high currents, likely resulting from its well-adhered metal–oxide interface and efficient gas release facilitated by its hierarchical structure (Qian et al., 2023; Xiang et al., 2024).

Underperforming Catalysts and Insights

Despite innovative designs, several catalysts underperformed:

- NiFeO/NiFe exhibited a high Tafel slope (104 mV dec^{-1}) and poor stability (5 h) (Gómez-Sacedón et al., 2024), likely due to surface passivation caused by dense oxide layers and insufficient structural integration (Nagappan et al., 2023).
- Ni–BDC–t/NF showed good kinetic performance but degraded after 11 h (Huang et al., 2024), implying that the organic linker might hydrolyze or leach under alkaline electrolysis conditions.
- P–NiFe@CF and Ni_2P@Ni–MOF/NF also displayed limited stabilities (8 h and 20 h, respectively) (H. Wang et al., 2021; Yun et al., 2021), despite decent Tafel slopes. This suggests that phosphidation on carbon fibers or MOFs may suffer from interfacial delamination or oxidative instability during prolonged UOR operation.

These findings underscore the importance of not only optimizing electronic configuration

and surface kinetics but also ensuring mechanical and chemical stability under realistic operating conditions.

Rational Design of a Future Catalyst Prototype

Based on the discussion in previous sections, an ideal future catalyst should possess the following features:

- Bimetallic or trimetallic composition, particularly incorporating elements such as Co, Ni, and Mo, which have demonstrated strong synergistic effects in enhancing urea oxidation kinetics and catalyst stability.
- Surface doping with non-metallic elements such as phosphorus (P) or sulfur (S) to tailor the electronic structure, increase surface reactivity, and expose more active sites.
- A highly porous nanosheet or nanofilm morphology, providing a large electrochemically active surface area and facilitating efficient diffusion of urea and OH^- ions.
- Chemically stable and conductive porous substrates, such as nickel foam or carbon-based materials, to support long-term operation under alkaline conditions and minimize performance degradation.
- Bifunctionality, enabling the catalyst to efficiently drive UOR at the anode and HER at the cathode, thereby simplifying cell design.

Conversely, the following characteristics should be avoided:

- Use of noble metals such as Ru and Pt, which, despite their high activity, present cost constraints and environmental concerns, making them less suitable for large-scale or sustainable applications.
- Overly complex layered composites lacking coherent charge-transport pathways, such as the BDC linker structure in Ni–BDC–t/NF, which may hinder electron mobility and reduce catalytic efficiency under practical conditions (i.e., avoid over-engineering materials).

Electrolyte Limitations: Idealized Electrolytes vs. Real Wastewater

Despite promising performance metrics, nearly all catalysts discussed in this review were evaluated in highly controlled and simplified electrolytes, typically 1 M KOH with ± 0.33–0.5 M urea, approximating the urea concentration in fresh urine (Akkari et al., 2025; Gnana kumar et al., 2020; Sanati et al., 2023). The use of KOH is primarily due to its strong alkalinity, which enhances ionic conductivity compared to NaOH or LiOH (Scibioh & Viswanathan, 2020). However, real wastewater contains not only urea but also a complex matrix of creatinine, uric acid, ammonium, phosphates, chlorides, sulfates, and various organic impurities, all of which may interfere with the electrochemical process (Akkari et al., 2025).

Furthermore, most studies employed analytical-grade urea (Alex et al., 2024; Dharmaraj et al., 2024; Fan et al., 2024; Gao et al., 2023; Gómez-Sacedón et al., 2024; Huang et al., 2024; Jin et al., 2024; X. Li et al., 2024; Ma et al., 2024; Miao et al., 2024; Parvin et al., 2024; Qian et al., 2023, 2024; Shaarawy et al., 2024; H. Wang et al., 2021; Y. Wang et al., 2023; Yang et al., 2024; Yun et al., 2021; Y. Zhao et al., 2024; Zhong et al., 2022) and overlooked the fact that urea is easily hydrolyzed by microbial urease, especially during storage or in untreated sewage. This presents a significant barrier to practical implementation, as urea rapidly decomposes into ammonia and CO_2, leading to fuel loss and pH alteration. Therefore, future systems must consider early-stage separation, chemical stabilization (e.g., pH conditioning using KOH), or direct electrolysis near the source, particularly in decentralized urine-diverting systems or specific industrial waste streams.

Wastewater Conditioning for Electrolyte Compatibility

To maintain urea as the active electrochemical species, real wastewater must undergo minimal yet strategic pretreatment. Effective approaches include filtration to remove particulates, alkaline stabilization (pH > 11) to suppress urease

activity, or the use of chemical inhibitors to delay urea hydrolysis (Randall et al., 2016; Svane et al., 2020). More advanced strategies, such as urea-selective membranes, could further enrich urea concentration while removing interfering species. These mild interventions preserve urea integrity without introducing excessive cost or complexity.

What Not to Do: Avoiding Urea-Depleting Treatments

Several conventional wastewater treatment processes are incompatible with urea electrolysis. Biological treatments such as activated sludge or UASB (upflow anaerobic sludge blanket) reactors rapidly degrade urea via enzymatic activity (Rahimi et al., 2020) and should therefore be avoided prior to electrolysis. Oxidative treatments employing strong chemical oxidants, such as ozone or sodium chlorate, that can break down urea should likewise be avoided (Urbańczyk et al., 2016). Similarly, ammonia stripping, nitrification–denitrification, and long-term storage without pH control may convert or remove urea (Urbańczyk et al., 2016; Zhou et al., 2023). Other processes, such as UV-AOPs, coagulation, and membrane separations, may destroy, bind, or exclude urea depending on their configuration (Urbańczyk et al., 2016). Consequently, a rethinking of treatment sequencing is necessary, placing electrolysis early in the treatment train or designing hybrid processes that preserve urea while simultaneously addressing other contaminants.

Conclusion

This review highlights the critical need for a systematic and performance-oriented evaluation of nickel-based electrocatalysts for urea electrolysis by bridging the gap between catalyst synthesis, structural design, and electrochemical performance. Unlike previous reviews that have primarily emphasized mechanistic insights, material characterization, or economic considerations, this work adopted a comparative framework grounded in standardized benchmarking conditions.

Through a thematic analysis of catalysts evaluated at current densities of 10, 50, 100, and 500 mA cm^{-2}, this study identified that an ideal catalyst should exhibit a bimetallic or trimetallic composition, a porous or hollow nanostructure, surface doping (e.g., phosphorus or sulfur), and a stable, conductive support material, while demonstrating bifunctional activity for both UOR and HER. Conversely, catalyst designs should avoid reliance on noble metals and excessively complex or poorly connected composite structures that impede charge transfer.

It is also important to emphasize that most catalysts discussed in this review were evaluated under controlled laboratory conditions using idealized alkaline electrolytes. Therefore, for successful real-world implementation, wastewater must be pretreated or conditioned to approximate the standardized electrolyte environment of 1 M KOH with approximately 0.33 M urea, in order to ensure compatibility and sustain catalytic performance.

References

Agrawal, P., Ebrahim, S., & Ponnamma, D. (2024). Advancements in nanocarbon-based catalysts for enhanced fuel cell performance: a comprehensive review. *International Journal of Energy and Water Resources*. https://doi.org/10.1007/s42108-024-00324-w

Akkari, S., Sánchez-Sánchez, C. M., Hopsort, G., Serrano, K. G., Loubière, K., Tzedakis, T., Benyahia, R., Rebiai, L., Bastide, S., Cachet-Vivier, C., Vivier, V., Lopez-Viveros, M., & Azimi, S. (2025). Progress on electrochemical and photoelectrochemical urea and ammonia conversion from urine for sustainable wastewater treatment. *Applied Catalysis B: Environment and Energy*, *362*, 124718. https://doi.org/10.1016/j.apcatb.2024.124718

Aladeemy, S. A., Arunachalam, P., Amer, M. S., & Al-Mayouf, A. M. (2025). Electrochemically embedded heterostructured Ni/NiS anchored onto carbon paper as bifunctional electrocatalysts for urea oxidation and hydrogen evolution reaction. *RSC Advances*, *15*(1), 14–25. https://doi.org/10.1039/D4RA07418A

Alex, C., Naduvil Kovilakath, M. S., Rao, N. N., Sathiskumar, C., Tayal, A., Meesala, L., Kumar, P., & John, N. S. (2024). In-situ generated Ni(OH)2 on chemically activated spent catalyst sustains urea electro-oxidation in extensive alkaline conditions. *International Journal of Hydrogen Energy*, *59*, 390–399. https://doi.org/10.1016/j.ijhydene.2024.01.339

Anuratha, K., Rinawati, M., Wu, T.-H., Yeh, M.-H., & Lin, J.-Y. (2022). Recent Development of Nickel-Based Electrocatalysts for Urea Electrolysis in Alkaline Solution. *Nanomaterials*, *12*(17), 2970. https://doi.org/10.3390/nano12172970

Ao, G.-H., Zhao, P.-Z., Peng, Z.-G., Wang, S., Guo, Y.-S., Chen, C.-T., & Wang, Z.-H. (2021). Construction of Hierarchical Porous Architecture on Ni Foam for Efficient Oxygen Evolution Reaction Electrode. *Frontiers in Materials*, *8*. https://doi.org/10.3389/fmats.2021.726270

Ao, X., Gu, Y., Li, C., Wu, Y., Wu, C., Xun, S., Nikiforov, A., Xu, C., Jia, J., Cai, W., Ma, R., Huo, K., & Wang, C. (2022). Sulfurization-functionalized 2D metal-organic frameworks for high-performance urea fuel cell. *Applied Catalysis B: Environmental*, *315*, 121586. https://doi.org/10.1016/j.apcatb.2022.121586

Bao, Y., Chen, K., Feng, Z., Ru, H., Guo, M., Chen, D., Li, X., Tu, J., Ding, L., & Lai, X. (2023). Bimetallic MoO 3 /Ni-N-C Nanoalloys Derived from MOFs for Electrocatalytic Urea Oxidation Reaction. *ACS Applied Nano Materials*, *6*(13), 11221–11229. https://doi.org/10.1021/acsanm.3c01258

Chen, K., Qian, J., Xu, W., & Li, T.-T. (2024). Hierarchical Superhydrophilic/Superaerophobic Ni(OH) 2 @NiFe-PBA Nanoarray Supported on Nickel Foam for Boosting the Oxygen Evolution Reaction. *Inorganic Chemistry*, *63*(1), 642–652. https://doi.org/10.1021/acs.inorgchem.3c03542

Chen, L., Wang, L., Ren, J., Wang, H., Tian, W., Sun, M., & Yuan, Z. (2024). Artificial Heterointerfaces with Regulated Charge Distribution of Ni Active Sites for Urea Oxidation Reaction. *Small Methods*, *8*(12). https://doi.org/10.1002/smtd.202400108

Chidunchi, I., Kulikov, M., Safarov, R., & Kopishev, E. (2024). Extraction of platinum group metals from catalytic converters. *Heliyon*, *10*(3), e25283. https://doi.org/10.1016/j.heliyon.2024.e25283

Da, Y., Jiang, R., Tian, Z., Han, X., Chen, W., & Hu, W. (2023). The applications of single-atom alloys in electrocatalysis: Progress and challenges. *SmartMat*, *4*(1). https://doi.org/10.1002/smm2.1136

Dharmaraj, K., Hanna, R., Lauermann, I., Bagacki, R., Xi, F., Kemppainen, E., Schlatmann, R., & Calnan, S. (2024). Electrodeposited Porous Nickel-Copper as a Non-Noble Metal Catalyst for Urea-Assisted Anion Exchange Membrane Electrolysis for Hydrogen Production. *ACS Sustainable Chemistry and Engineering*, *12*(26), 9908–9921. https://doi.org/10.1021/acssuschemeng.4c02424

Fan, X., Fu, Z., Lin, J., He, B., Zhang, J., Hu, E., & Chen, Z. (2024). Modulation of energy barrier of reaction steps over S-doped Ni(OH)2/Cu composites to achieve high-performance urea electrolysis catalysts. *Chemical Engineering Journal*, *490*. https://doi.org/10.1016/j.cej.2024.151251

Gao, X., Bai, X., Wang, P., Jiao, Y., Davey, K., Zheng, Y., & Qiao, S. Z. (2023). Boosting urea electrooxidation on oxyanion-engineered nickel sites via inhibited water oxidation. *Nature Communications*, *14*(1).

https://doi.org/10.1038/s41467-023-41588-w

Gaur, A., John, J. M., Pundir, V., Kaur, R., & Bagchi, V. (2023). Electronegativity-Induced Valence State Augmentation of Ni and Co through Electronic Redistribution between Co-Ni 3 N/CeF 3 Interfaces for Oxygen Evolution Reaction. *ACS Applied Energy Materials*, *6*(3), 1763–1770. https://doi.org/10.1021/acsaem.2c03656

Ge, J., Kuang, J., Xiao, Y., Guan, M., & Yang, C. (2023). Recent development of nickel-based catalysts and in situ characterization techniques for mechanism understanding of the urea oxidation reaction. *Surfaces and Interfaces*, *41*, 103230. https://doi.org/10.1016/j.surfin.2023.103230

Ghosh, A., Fathima Thanutty Kallungal, S., & Ramaprabhu, S. (2023). 2D Metal-Organic Frameworks: Properties, Synthesis, and Applications in Electrochemical and Optical Biosensors. *Biosensors*, *13*(1), 123. https://doi.org/10.3390/bios13010123

Gnana kumar, G., Farithkhan, A., & Manthiram, A. (2020). Direct Urea Fuel Cells: Recent Progress and Critical Challenges of Urea Oxidation Electrocatalysis. *Advanced Energy and Sustainability Research*, *1*(1). https://doi.org/10.1002/aesr.202000015

Gómez-Sacedón, C., López-Fernández, E., González-Elipe, A. R., Espinós, J. P., Yubero, F., Gil-Rostra, J., & de Lucas-Consuegra, A. (2024). NiFeO/NiFe bilayer electrocatalyst for an efficient urea assisted water electrolysis. *International Journal of Hydrogen Energy*, *59*, 604–613. https://doi.org/10.1016/j.ijhydene.2024.02.079

Huang, L., Li, N., Xiao, J., Lou, H., Xie, C., Yang, Y., Jiang, H., & Zhang, W. (2024). Morphology-controlled nickel-organic framework nanosheet arrays for efficient urea electrolysis in alkaline media. *Journal of Electroanalytical Chemistry*, *965*. https://doi.org/10.1016/j.jelechem.2024.118363

Hu, X., Tian, X., Lin, Y.-W., & Wang, Z. (2019). Nickel foam and stainless steel mesh as electrocatalysts for hydrogen evolution reaction, oxygen evolution reaction and overall water splitting in alkaline media. *RSC Advances*, *9*(54), 31563–31571. https://doi.org/10.1039/C9RA07258F

Isik, I. B., Kaya, D., Isik, H. H., Ekicibil, A., & Karadag, F. (2024). Bifunctional bimetallic PtNi, PtCu, and NiCu nanoparticles: Electrocatalytic activities for hydrogen evolution reaction and magnetic properties. *Materials Science and Engineering: B*, *300*, 117081. https://doi.org/10.1016/j.mseb.2023.117081

Islam Rubel, R., Hasan Ali, Md., Abu Jafor, Md., & Mahmodul Alam, Md. (2019). Carbon nanotubes agglomeration in reinforced composites: A review. *AIMS Materials Science*, *6*(5), 756–780. https://doi.org/10.3934/matersci.2019.5.756

Jin, H., Yu, L., Xiong, K., Chen, J., Zhang, H., Deng, M., & Shi, X. (2024). An energy-efficient H2 production based on urea-aided water splitting enhanced by Ru induced in-situ speciation of NiO nanosheets on porous Ni. *Journal of Alloys and Compounds*, *983*. https://doi.org/10.1016/j.jallcom.2024.173938

Ji, X., Zhang, Y., Ma, Z., & Qiu, Y. (2020). Oxygen Vacancy-rich Ni/NiO@NC Nanosheets with Schottky Heterointerface for Efficient Urea Oxidation Reaction. *ChemSusChem*, *13*(18), 5004–5014. https://doi.org/10.1002/cssc.202001185

Ke, J., He, F., Wu, H., Lyu, S., Liu, J., Yang, B., Li, Z., Zhang, Q., Chen, J., Lei, L., Hou, Y., & Ostrikov, K. (2021). Nanocarbon-Enhanced 2D Photoelectrodes: A New Paradigm in Photoelectrochemical Water Splitting. *Nano-Micro Letters*, *13*(1), 24. https://doi.org/10.1007/s40820-020-00545-8

Li, J., Zhang, J., & Yang, J.-H. (2022). Research progress and applications of nickel-based catalysts for electrooxidation of urea. *International Journal of Hydrogen Energy*, *47*(12), 7693–7712.

https://doi.org/10.1016/j.ijhydene.2021.12.099

Li, L., Soyhan, I., Warszawik, E., & van Rijn, P. (2024). Layered Double Hydroxides: Recent Progress and Promising Perspectives Toward Biomedical Applications. *Advanced Science*, *11*(20). https://doi.org/10.1002/advs.202306035

Liu, Y., Chen, Y., Liang, C., Liang, Z., Fan, C., Wang, F., & Lei, J. (2024). Low-Pt-loading electrocatalyst derived from the reduction of hydrogenated MoO3 for highly efficient hydrogen evolution reaction. *International Journal of Hydrogen Energy*, *51*, 701–708. https://doi.org/10.1016/j.ijhydene.2023.10.179

Li, W., Cheng, G., Peng, S., Sun, M., Wang, S., Han, S., Liu, Y., Zhai, T., & Yu, L. (2022). Tuning hydrogen binding energy by interfacial charge transfer enables pH-universal hydrogen evolution catalysis of metal phosphides. *Chemical Engineering Journal*, *430*, 132699. https://doi.org/10.1016/j.cej.2021.132699

Li, X., Wang, Y., Du, X., & Zhang, X. (2024). Controlled synthesis of X (X = Mo, Cr and W) doped NiCoP nanostructures as efficient and environmentally friendly urea electrolysis catalyst. *Fuel*, *365*. https://doi.org/10.1016/j.fuel.2024.131219

Li, X., Zhao, L., Yu, J., Liu, X., Zhang, X., Liu, H., & Zhou, W. (2020). Water Splitting: From Electrode to Green Energy System. *Nano-Micro Letters*, *12*(1), 131. https://doi.org/10.1007/s40820-020-00469-3

Ma, D., Jia, Y., Li, Y., Yang, H., Wang, F., Zheng, X., Shao, G., Xiong, Q., Shen, Z., Liu, M., Lou, Z., & Gu, C. (2024). Anion modulate the morphological and electronic structure of NiFe-based electrocatalyst for efficient urea oxidation-assisted water electrolysis. *Journal of Materials Science and Technology*, *197*, 207–214. https://doi.org/10.1016/j.jmst.2024.01.054

Masjedi, S. K., Kazemi, A., Moeinnadini, M., Khaki, E., & Olsen, S. I. (2024). Urea production: An absolute environmental sustainability assessment. *Science of The Total Environment*, *908*, 168225. https://doi.org/10.1016/j.scitotenv.2023.168225

Miao, J., Hong, Q. L., Zhang, P., Ren, Z. F., Zhao, A. C., Li, Y. H., Wang, P. F., & Chen, Y. (2024). Self-supported Pt nanoparticles-NiFeP nanosheets arrays nanohybrid with hydrophilic surface towards urea electrolysis. *Applied Surface Science*, *652*. https://doi.org/10.1016/j.apsusc.2023.159276

Moriau, L., Bele, M., Marinko, Ž., Ruiz-Zepeda, F., Koderman Podboršek, G., Šala, M., Šurca, A. K., Kovač, J., Arčon, I., Jovanovič, P., Hodnik, N., & Suhadolnik, L. (2021). Effect of the Morphology of the High-Surface-Area Support on the Performance of the Oxygen-Evolution Reaction for Iridium Nanoparticles. *ACS Catalysis*, *11*(2), 670–681. https://doi.org/10.1021/acscatal.0c04741

Nagappan, S., Yang, S., Adhikari, A., Patel, R., & Kundu, S. (2023). A review on consequences of flexible layered double hydroxide-based electrodes: fabrication and water splitting application. *Sustainable Energy & Fuels*, *7*(16), 3741–3775. https://doi.org/10.1039/D3SE00573A

Niu, H., Wang, Q., Huang, C., Zhang, M., Yan, Y., Liu, T., & Zhou, W. (2023). Noble Metal-Based Heterogeneous Catalysts for Electrochemical Hydrogen Evolution Reaction. *Applied Sciences*, *13*(4), 2177. https://doi.org/10.3390/app13042177

Parvin, S., Aransiola, E., Ammar, M., Lee, S., Zhang, L., Weber, J., & Baltrusaitis, J. (2024). Tailored Ni(OH)2/CuCo/Ni(OH)2 Composite Interfaces for Efficient and Durable Urea Oxidation Reaction. *ACS Applied Materials and Interfaces*. https://doi.org/10.1021/acsami.4c14041

Patel, K. B., Parmar, B., Ravi, K., Patidar, R., Chaudhari, J. C., Srivastava, D. N., & Bhadu, G. R. (2023). Metal-organic framework derived core-shell nanoparticles as high performance bifunctional electrocatalysts for HER and OER. *Applied Surface Science*, *616*,

156499. https://doi.org/10.1016/j.apsusc.2023.156499

Poimenidis, I. A., Papakosta, N., Klini, A., Farsari, M., Konsolakis, M., Loukakos, P. A., & Moustaizis, S. D. (2023). Electrodeposited Ni foam electrodes for increased hydrogen production in alkaline electrolysis. *Fuel*, *342*, 127798. https://doi.org/10.1016/j.fuel.2023.127798

Putri, L. K., Ng, B.-J., Yeo, R. Y. Z., Ong, W.-J., Mohamed, A. R., & Chai, S.-P. (2023). Engineering nickel phosphides for electrocatalytic hydrogen evolution: A doping perspective. *Chemical Engineering Journal*, *461*, 141845. https://doi.org/10.1016/j.cej.2023.141845

Qian, G., Chen, J., Jiang, W., Yu, T., Tan, K., & Yin, S. (2023). Strong electronic coupling of CoNi and N-doped-carbon for efficient urea-assisted H2 production at a large current density. *Carbon Energy*, *5*(12). https://doi.org/10.1002/cey2.368

Qian, G., Lu, T., Wang, Y., Xu, H., Cao, X., Xie, Z., Chen, C., & Min, D. (2024). N-induced compressive strain in Ni-MoO2 heterostructure with micro-nano array for improving high-current-output urea-assisted water electrolysis performance. *Chemical Engineering Journal*, *480*. https://doi.org/10.1016/j.cej.2023.147993

Qiao, P., Li, G., Xu, X., Wang, D., Wang, F., Xu, L., Lu, L., Cong, H., & Sun, M. (2024). Mediating Self-Oxidation and Competitive Adsorption for Achieving High-Selective Urea Oxidation Catalysis at Industrial-Level Current Densities. *Advanced Functional Materials*. https://doi.org/10.1002/adfm.202421136

Qu, J., Dong, Y., Zhang, T., Zhao, C., Wei, L., & Guan, X. (2024). Impact of bimetallic synergies on Mo-doping NiFeOOH: Insights into enhanced OER activity and reconstructed electronic structure. *Frontiers in Energy*, *18*(6), 850–862. https://doi.org/10.1007/s11708-024-0960-6

Rahimi, S., Modin, O., & Mijakovic, I. (2020). Technologies for biological removal and recovery of nitrogen from wastewater. *Biotechnology Advances*, *43*, 107570. https://doi.org/10.1016/j.biotechadv.2020.107570

Randall, D. G., Krähenbühl, M., Köpping, I., Larsen, T. A., & Udert, K. M. (2016). A novel approach for stabilizing fresh urine by calcium hydroxide addition. *Water Research*, *95*, 361–369. https://doi.org/10.1016/j.watres.2016.03.007

Ratsoma, M. S., Poho, B. L. O., Makgopa, K., Raju, K., Modibane, K. D., Jafta, C. J., & Oyedotun, K. O. (2023). Application of Nickel Foam in Electrochemical Systems: A Review. *Journal of Electronic Materials*, *52*(4), 2264–2291. https://doi.org/10.1007/s11664-023-10244-w

Sanati, S., Morsali, A., & García, H. (2023). Metal-organic framework-based materials as key components in electrocatalytic oxidation and reduction reactions. *Journal of Energy Chemistry*, *87*, 540–567. https://doi.org/10.1016/j.jechem.2023.08.042

Santos, H. L. S., Corradini, P. G., Medina, M., Dias, J. A., & Mascaro, L. H. (2020). NiMo–NiCu Inexpensive Composite with High Activity for Hydrogen Evolution Reaction. *ACS Applied Materials & Interfaces*, *12*(15), 17492–17501. https://doi.org/10.1021/acsami.0c00262

Scibioh, M. A., & Viswanathan, B. (2020). Electrolyte materials for supercapacitors. In *Materials for Supercapacitor Applications* (pp. 205–314). Elsevier. https://doi.org/10.1016/B978-0-12-819858-2.00004-4

Seo, D.-G., Park, D.-H., Park, S.-H., Gu, Y., Lim, D.-M., Hong, C.-E., Han, J.-I., Kim, J.-H., Jang, J.-S., Kim, E.-J., Yun, J.-W., Jo, H.-M., & Park, K.-W. (2025). Optimization of hollow Pt-Ni alloy bifunctional electrocatalysts via ethylene glycol/glycerol ratio in modified polyol process. *Journal of Power Sources*, *632*, 236322. https://doi.org/10.1016/j.jpowsour.2025.236322

Shaarawy, H. H., Hussein, H. S., Attia, A., & Hawash, S. I. (2024). Green hydrogen generation in alkaline solution using electrodeposited Ni-Co-nano-graphene thin film cathode. *Environmental Science and Pollution Research*, *31*(19), 28719–28733. https://doi.org/10.1007/s11356-024-32948-0

Shaban, A., Basiouny, M. E., & AboSiada, O. A. (2024). Comparative study of the removal of urea by electrocoagulation and electrocoagulation combined with chemical coagulation in aqueous effluents. *Scientific Reports*, *14*(1), 30605. https://doi.org/10.1038/s41598-024-81422-x

Su, L., Cui, X., He, T., Zeng, L., Tian, H., Song, Y., Qi, K., & Xia, B. Y. (2019). Surface reconstruction of cobalt phosphide nanosheets by electrochemical activation for enhanced hydrogen evolution in alkaline solution. *Chemical Science*, *10*(7), 2019–2024. https://doi.org/10.1039/C8SC04589E

Svane, S., Sigurdarson, J. J., Finkenwirth, F., Eitinger, T., & Karring, H. (2020). Inhibition of urease activity by different compounds provides insight into the modulation and association of bacterial nickel import and ureolysis. *Scientific Reports*, *10*(1), 8503. https://doi.org/10.1038/s41598-020-65107-9

Tumiwa, J. R., & Mizik, T. (2025). Advancing nickel-based catalysts for enhanced hydrogen production: Innovations in electrolysis and catalyst design. *International Journal of Hydrogen Energy*, *109*, 961–978. https://doi.org/10.1016/j.ijhydene.2025.02.020

Tutar, R., Ceylan, D., & Çelebi-Saltik, B. (2024). Preparation and characterization of conductive and multi-network nanocomposite hydrogels as potential scaffolds for electroactive tissues. *New Journal of Chemistry*, *48*(33), 14736–14745. https://doi.org/10.1039/D4NJ01930J

Urbańczyk, E., Sowa, M., & Simka, W. (2016). Urea removal from aqueous solutions—a review. *Journal of Applied Electrochemistry*, *46*(10), 1011–1029. https://doi.org/10.1007/s10800-016-0993-6

Vij, V., Sultan, S., Harzandi, A. M., Meena, A., Tiwari, J. N., Lee, W.-G., Yoon, T., & Kim, K. S. (2017). Nickel-Based Electrocatalysts for Energy-Related Applications: Oxygen Reduction, Oxygen Evolution, and Hydrogen Evolution Reactions. *ACS Catalysis*, *7*(10), 7196–7225. https://doi.org/10.1021/acscatal.7b01800

Wallnöfer-Ogris, E., Grimmer, I., Ranz, M., Höglinger, M., Kartusch, S., Rauh, J., Macherhammer, M.-G., Grabner, B., & Trattner, A. (2024). A review on understanding and identifying degradation mechanisms in PEM water electrolysis cells: Insights for stack application, development, and research. *International Journal of Hydrogen Energy*, *65*, 381–397. https://doi.org/10.1016/j.ijhydene.2024.04.017

Wang, G., Li, X., Wang, J., Yan, H., Zhang, D., Tian, C., Zhang, H., & Jiao, Y. (2025). Vanadium-Modulated Molybdenum/Nickel-Based Multi-Heterostructures finely tailoring d-Band centers for electrocatalytic water splitting. *Journal of Colloid and Interface Science*, 137543. https://doi.org/10.1016/j.jcis.2025.137543

Wang, H., Zou, H., Liu, Y., Liu, Z., Sun, W., Lin, K. A., Li, T., & Luo, S. (2021). Ni2P nanocrystals embedded Ni-MOF nanosheets supported on nickel foam as bifunctional electrocatalyst for urea electrolysis. *Scientific Reports*, *11*(1). https://doi.org/10.1038/s41598-021-00776-8

Wang, Y., Lu, Y., Shi, Y., Wang, J., Zheng, Y., Pan, J., Li, C., & Cao, J. (2023). Realizing highly-efficient urea oxidation via decreasing the energy barrier of deprotonation over regulated electronic structure of Co doped Ni(OH)2. *Applied Surface Science*, *640*. https://doi.org/10.1016/j.apsusc.2023.158391

Weerakoon, D., Bansal, B., Padhye, L. P., Rachmani, A., James Wright, L., Silyn Roberts, G., & Baroutian, S. (2023). A

critical review on current urea removal technologies from water: An approach for pollution prevention and resource recovery. *Separation and Purification Technology*, *314*, 123652. https://doi.org/10.1016/j.seppur.2023.123652

Wu, T.-H., Lin, Y.-C., Hou, B.-W., & Liang, W.-Y. (2020). Nanostructured β−NiS Catalyst for Enhanced and Stable Electro−oxidation of Urea. *Catalysts*, *10*(11), 1280. https://doi.org/10.3390/catal10111280

Xiang, R., Yu, Y., Wang, C., & Gao, Q. (2024). Construction of hierarchical CoNiMoOxHy/NF nanostructures for highly efficient urea oxidation reaction. *Electrochimica Acta*, *479*, 143832. https://doi.org/10.1016/j.electacta.2024.143832

Yang, D., Li, J., Li, W., Jiao, Y. Z., & Yang, J. H. (2024). The ultrathin regular circular structural Ni-P nanosheet for efficient urea electrooxidation. *Journal of Environmental Chemical Engineering*, *12*(2). https://doi.org/10.1016/j.jece.2024.112433

Yu, F.-Y., Lang, Z.-L., Yin, L.-Y., Feng, K., Xia, Y.-J., Tan, H.-Q., Zhu, H.-T., Zhong, J., Kang, Z.-H., & Li, Y.-G. (2020). Pt-O bond as an active site superior to Pt0 in hydrogen evolution reaction. *Nature Communications*, *11*(1), 490. https://doi.org/10.1038/s41467-019-14274-z

Yun, W. H., Das, G., Kim, B., Park, B. J., Yoon, H. H., & Yoon, Y. S. (2021). Ni–Fe phosphide deposited carbon felt as free-standing bifunctional catalyst electrode for urea electrolysis. *Scientific Reports*, *11*(1). https://doi.org/10.1038/s41598-021-01383-3

Zhao, Q., Meng, C., Kong, D., Wang, Y., Hu, H., Chen, X., Han, Y., Chen, X., Zhou, Y., Lin, M., & Wu, M. (2021). In Situ Construction of Nickel Sulfide Nano-Heterostructures for Highly Efficient Overall Urea Electrolysis. *ACS Sustainable Chemistry & Engineering*, *9*(46), 15582–15590. https://doi.org/10.1021/acssuschemeng.1c05722

Zhao, Y., Zhou, P., Li, Z., Zhao, B., Jiang, W., Chen, X., Wang, J., Yang, R., & Zuo, C. (2024). Interfacial engineering of hierarchical MoNi4/NiO heterostructure nanosheet arrays as bifunctional electrocatalysts for urea-assisted energy-saving hydrogen production. *Colloids and Surfaces A: Physicochemical and Engineering Aspects*, *681*. https://doi.org/10.1016/j.colsurfa.2023.132776

Zhong, M., Li, W., Wang, C., & Lu, X. (2022). Synthesis of hierarchical nickel sulfide nanotubes for highly efficient electrocatalytic urea oxidation. *Applied Surface Science*, *575*. https://doi.org/10.1016/j.apsusc.2021.151708

Zhou, Y., Zhu, Y., Zhu, J., Li, C., & Chen, G. (2023). A Comprehensive Review on Wastewater Nitrogen Removal and Its Recovery Processes. *International Journal of Environmental Research and Public Health*, *20*(4), 3429. https://doi.org/10.3390/ijerph20043429.